

Microstructure evaluation of an advanced high strength steel with superior results in terms of strength-ductility trade-off

Tairine Berbert Tavares ^{1*} Fernando de Souza Costa ¹Marília Faria de Oliveira Caizer ¹

Abstract

Major improvements in new advanced high strength steels, especially related to microstructural features, have been made by the steel sector to access the trade-off between strength and ductility. In this context, the present study provides a detailed analysis of the microstructure of a cold rolled steel with a minimum tensile strength of 980 MPa, which possesses superior elongation when compared to other conceptions of steels from the same strength level. The annealing process was simulated in a Gleeble machine, and the microstructural characterization was done using optical and scanning electron microscopy, EBSD and XRD analysis. Austenite decomposition, using dilatometric test, and mechanical properties were also evaluated. The steel characterization revealed a microstructure consisting of ferrite matrix with martensite islands and retained austenite particles, in a fraction equivalent to that of conventional TRIP steels, dispersed throughout. The carbon content in the austenite, however, was less than 1.0% w/w, which results in a relatively low stability. Therefore, the increase in strain hardening capacity enabled by the deformation-induced transformation of austenite to martensite produces increased ductility during straining, distinguishing the analyzed material from other steels of the same strength level.

Keywords: Advanced high strength steel; Microstructure; Strength-ductility trade-off; TRIP effect.

1 Introduction

For a long time, steel has been used as the dominant material in the car construction, corresponding to approximately 60% of the weight of an average automobile. Through this usage, high levels of safety and desired standards of strength are guaranteed at relatively low costs. However, given the increasing pressure for more fuel-efficient cars, due to the stringent regulations pertaining to energy consumption and air pollution, reducing the weight of the carbody has become an extremely important consideration for the automotive sector. As a response, advanced high strength steels (AHSS) have been developed by the steel industry in order to meet these recent requirements. These high-performance steels are basically related to multiphase microstructures with improved strength and formability characteristics [1-5].

The third generation of AHSS is currently ongoing. In this case, the good combination of properties has been achieved by the employment of the transformation-induced plasticity (TRIP) effect, where the metastable austenite contributes to the strain hardening capacity of the steel through its transformation to martensite during straining, resulting in a delay of necking and, as a consequence, improving the elongation. The excellent strength-ductility balance reached through this beneficial phenomenon allows, therefore, the usage of these steels in thinner structural parts, with the consequent reduction of the automobile weight [5-7].

Seeking to meet the demand for steels with both higher strength and higher ductility, research works were done at Usiminas, a steel company in Brazil leader in the manufacturing and commercialization of steel sheets, in order to design a new steel sheet with a minimum tensile strength of 980 MPa and superior elongation when compared to other conceptions of steels with the same strength level. The current work provides a detailed analysis of the microstructure of the referred steel, produced through continuous annealing process simulation in a Gleeble machine.

As a result, the present work summarizes the main results obtained in the referred research, in which a steel for applications where a combination of good formability and strength is of interest was developed. Firstly, the processing parameters applied at a Gleeble thermomechanical simulator to obtain the referred steel will be presented, which simulates the thermal cycle commonly applied at Usiminas' continuous annealing line. Then, a detailed analysis of the microstructure through more than one characterization method will be discussed. Subsequently, the austenite decomposition into ferrite and other transformation products, based on the mentioned thermal cycle, will be analyzed through dilatometric tests. Finally, the steel's properties will be overviewed.

¹Centro de Pesquisa e Desenvolvimento, Usiminas, Ipatinga, MG, Brasil.

*Corresponding author: tairine.tavares@usiminas.com



2 Materials and methods

Sheets of an industrially produced cold rolled (0.30C-2.50Mn-2.20Si max. wt. %) steel, having 1.1 mm thickness, were used for this study. The continuous annealing cycle, with an intercritical temperature of T_1 , where $700\text{ }^\circ\text{C} < T_1 < 850\text{ }^\circ\text{C}$, was simulated at a Gleeble thermomechanical simulator, using a sample with $50 \times 150 \times 1.1\text{ mm}$ dimensions, with the length aligned to the rolling direction. This temperature range was chosen in order to simulate the processing parameters usually applied in the Usiminas' continuous annealing line. Figure 1 shows a schematic diagram of the thermal cycle applied.

The transition temperatures Ac_1 and Ac_3 , as well as the volume fraction of austenite achieved at the end of the soaking step through lever rule, and the austenite decomposition into ferrite and other transformation products were evaluated through dilatometric tests conducted in a Bähr DIL805 A/D dilatometer. For this analysis, the test pieces were cut out from the cold rolled sheet in a rectangular geometry: $4 \times 10 \times 1.1\text{ mm}$.

The samples were heated at a constant rate of t_1 ($< 10\text{ }^\circ\text{C/s}$) until T_1 , held at this temperature for approximately

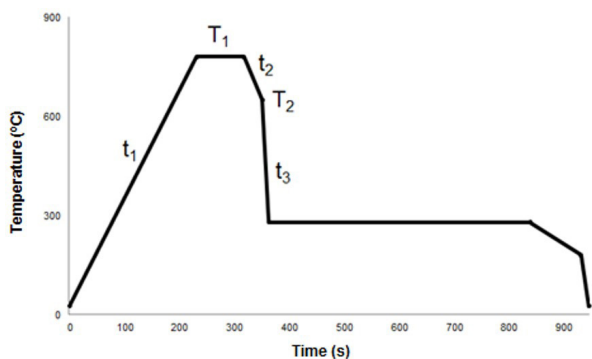


Figure 1. Schematic diagram of the thermal cycle simulated on Gleeble according to the Usiminas' continuous annealing line.

80 s, cooled to T_2 at t_2 ($< 10\text{ }^\circ\text{C/s}$), and then cooled to room temperature at t_3 ($> 30\text{ }^\circ\text{C/s}$).

The microstructural characterization was carried out in the annealed state using an optical microscope (OM), a field emission scanning electron microscope (FESEM) and electron backscattering diffraction (EBSD). For the OM and SEM analysis, the specimens were mechanically ground and polished to a mirror-like surface, with diamond paste, applying standard metallographic techniques. Subsequently, 4% and 2% nital etchants were used to reveal the microstructure. Beyond that, for the EBSD examination, it was used a scan step size of $0.15\text{ }\mu\text{m}$ and an accelerating voltage of 20 kV, at 1/4 of the sample thickness, after additional final polishing using diamond solution of $0.1\text{ }\mu\text{m}$ and colloidal silica particles. The diffraction data were post-processed using the Oxford HKL acquisition and analysis software.

X-ray diffraction (XRD) measurements were performed at room temperature in a Bruker D8 Advance diffractometer, working in vertical Bragg–Brentano geometry and using $\text{Co-K}\alpha$ radiation ($\lambda = 0.179\text{ nm}$), with a diffraction angle varying from 4° to 70° , and a step size of 0.02°s^{-1} .

In order to evaluate the mechanical behavior of the steel, uniaxial tensile tests were performed parallel to the rolling direction, using an Instron 5882 machine, at room temperature. Tensile test specimens were machined according to the subsize dimensions established by ASTM A370 standard [8] with gage dimension of $25 \times 6.25\text{ mm}$, respecting the sample thickness. The results were determined as an average of three specimens tested.

3 Results and discussion

3.1 Microstructural analyses

Examples of the SEM micrographs obtained for the steel sample produced in this work are presented in Figure 2.

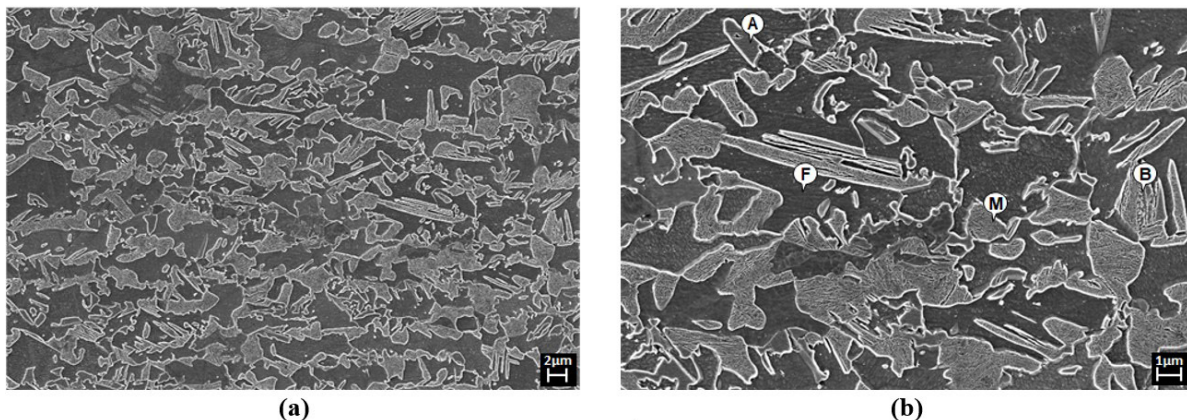


Figure 2. SEM micrographs of the analyzed condition showing (a) the phases' distribution and (b) the microstructural constituents. A: austenite, B: bainite, F: ferrite, M: martensite.

The images show a homogeneous microstructure, with the presence of hard-phase structures consisting of martensite and some bainite, and a significant amount of retained austenite particles in a matrix of ferrite grains. These are the features expected in the final microstructure to achieve the desired properties, since the retained austenite, even in small fractions, contributes to the increase of ductility due to the TRIP effect, and the martensite phase ensures the strength of the material due to its higher hardness.

The XRD pattern (Figure 3) revealed that the average volume fraction of retained austenite, calculated through the Rietveld method, was similar to the value found in conventional TRIP steels, around 11%. On the other hand, its carbon content of 0.81% w/w was lower than the value usually observed in those steels, which tends to be greater than 1.0% w/w. As a consequence, in this case, the austenite originated from the annealing cycle has a lower stability, so that during straining it tends to rapidly transform into martensite, providing some increase of ductility through the transformation induced plasticity (TRIP) effect, but in a more discrete degree.

It is known that the observed partial replacement of martensite by bainite can result in a decrease of the strengthening capacity. However, the volume fraction of bainite was so small (1.3% of the total microstructure, according to the manual point counting method [9]) that it was not capable of negatively affecting the steel properties. In fact, the strain hardening exponent, or n value, remained around 0.2. This high n value stabilizes the tensile deformation against the local instability, resulting in higher uniform elongation [10].

It is worth mentioning that conventional diffraction-based methods, like XRD, consider the difference in lattice symmetry to determine the phase volume fraction of each steel constituent. In this case, phases with almost identical lattice structures, such as martensite and ferrite, are difficult

to discriminate, resulting in a broadening of the α phase peaks, as shown in the remaining 88.94%. This situation happens because the body-centered tetragonal lattice of martensite generally shows little difference from the body-centered cubic lattice of ferrite, which makes it difficult to measure the volume fraction of each phase with reasonable accuracy [5,7].

For the same reason, analysis through EBSD also has its limitations when considering the symmetry of the pattern. However, a quantitative measure of the pattern quality is very useful for presenting images of microstructures, since it is sensitive to lattice defects and surface topology, and it can also present phase contrast, since different phases generally have different diffraction intensities [7]. Considering a grayscale, where the contrast ranges from black (0 value), at the weakest intensity, to white (255 value) at the strongest, a high-quality pattern shows, then, high values of the signal intensities, represented by the components band slope (BS) and band contrast (BC). On the other hand, as the microconstituents that form at low temperatures, such as martensite and bainite, normally have higher dislocation density, they emit poorer quality patterns than ferrite, leading to degraded EBSD patterns, and then, having lower band slope values [3,11].

Thus, in the EBSD maps, illustrated in Figure 4, the phase analysis was performed through BS and BC signals. As can be seen through the BC map (Figure 4a), the difference between ferrite and martensite is not clearly exhibited. However, along with the BS map (Figure 4b), the characteristics of the steel structure is shown with a relatively strong image contrast. In this case, the ferrite grain boundaries and the phases with a high degree of lattice imperfections are revealed by darker tones, as they have low BS values. Through this result, the bimodal distribution of the image quality (IQ) profile (Figure 4d) obtained from the measured sample area in Figure 4b can be used to estimate the phase

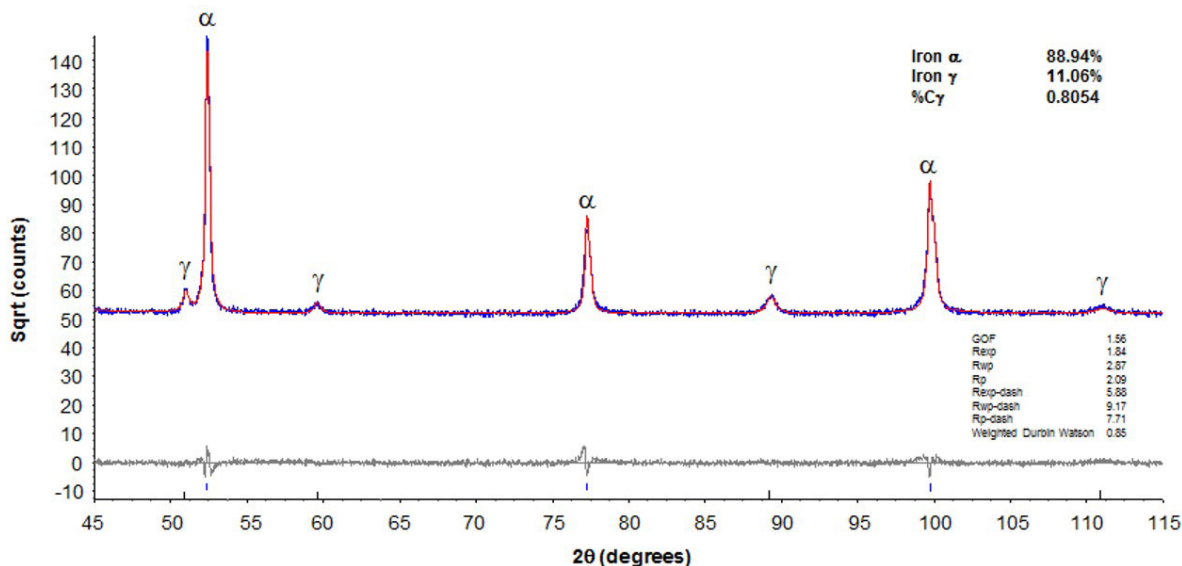


Figure 3. XRD pattern of the specimen analyzed.

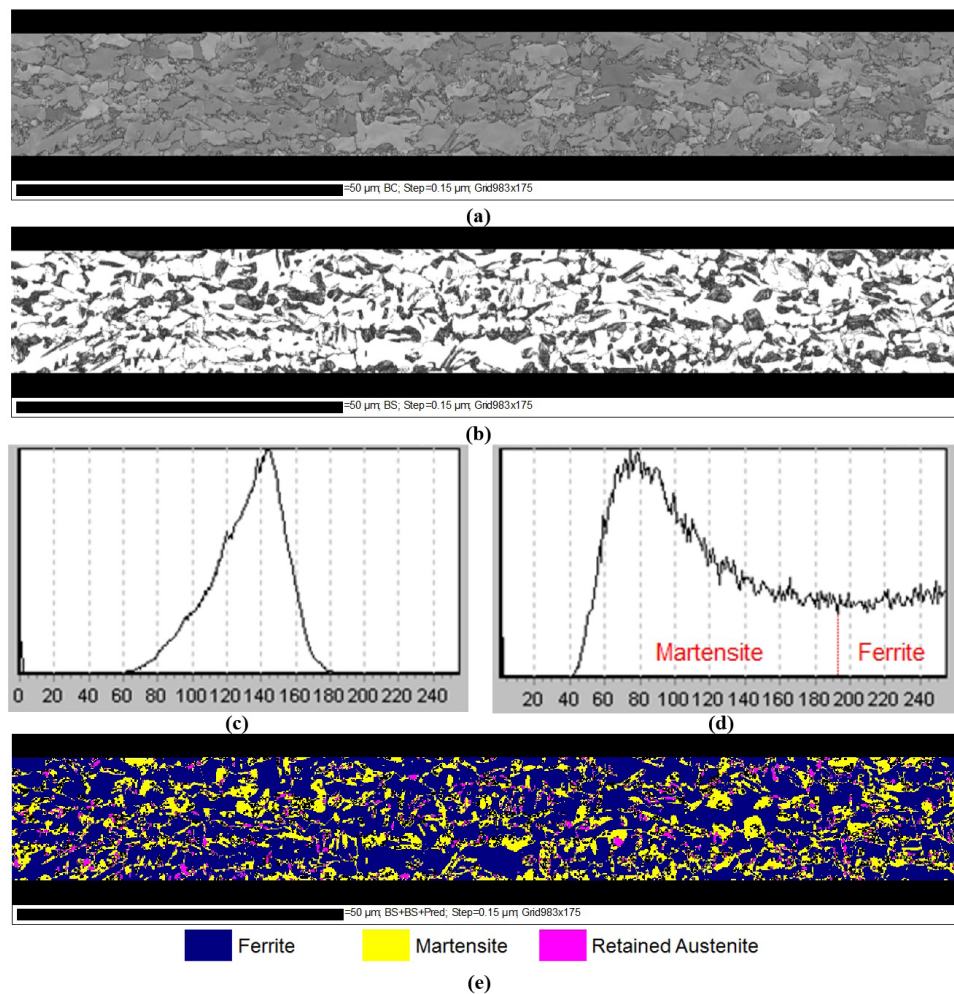


Figure 4. Steel microstructure revealed by electron backscatter diffraction (EBSD): (a) band contrast (BC) map, (b) band slope (BS) map, (c) profile of BC, (d) profile of BS, and (e) reconstructed phase map overlaid on BC map.

volume fraction. As previously mentioned, considering bainite negligible, an appropriate threshold can be chosen at the valley around 195, where values higher than this threshold, in the right side of the IQ profile, correspond to ferrite, and values between 0 and 194, martensite. As indicated by Wilson and coauthors [12], setting the threshold at the valley between these two phases seems a reasonable choice since this is the point where the contribution due to ferrite bends the curve back upward. The resulting volume fraction of each phase was 27.3% of martensite and 68.7% of ferrite, which was quite close to the result obtained by the manual point counting method, 29.8% and 62.4%, respectively. Figure 4e shows the phases distribution evaluation through EBSD, where the blue regions represent ferrite, and the yellow ones, martensite.

Regarding the retained austenite, represented by pink in Figure 4e, the automated analysis, obtained directly from the EBSD software as a result of its different crystallographic structure (*face-centered cubic lattice*), revealed a volume fraction equivalent to 4.1%, differently from the 11% value observed via XRD. This difference is probably related to the

spatial resolution limit of the SEM, to the smaller area of EBSD analysis, and to the deformation induced transformation of the less stable austenite into martensite during the sample preparation, all of which would result in an underestimation of the volume fraction value. In the last case, alternative specimen preparation methods may improve the results, but it is a problem difficult to overcome. Moreover, X-ray measurements are supposed to suffer from the same issue but to a lesser extent, since its penetration below the surface is considerably greater [13].

The dissociation of the BS profile into Gaussian peaks, where each peak represents a different phase [14], revealed that the spatial distribution is better described by three distinct peaks of the function, as shown in Figure 5.

Since the micrographs did not show a considerable amount of bainite, the lower BS part, which is described by two separable peaks, probably indicate the duplex nature of the martensitic islands, and the peak in the region of high BS values corresponds to the ferrite matrix. Kang et al. [11], in their study about phase determination, described the characteristics of the two kinds of martensite

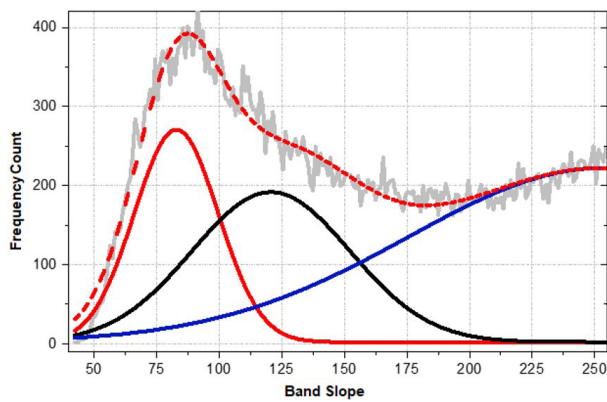


Figure 5. Profile of BS with Gaussian distribution analysis.

found in an AHSS. According to the authors, the martensite island in a BC image consists of both darker and relatively brighter areas, which correspond to twinned and twin-free sub-volumes, respectively. The twinned martensite forms at lower temperatures and contains numerous fine twins combined with a high density of dislocations. As a result, it presents a more degraded EBSD pattern quality when compared to the so-called twin-free dislocated martensite.

In addition to the previous results, the fraction of transformed products estimated through dilatometric tests using the lever rule between Ac_3 and Ac_1 is represented in Figure 6. It is possible to notice that the starting and finishing transformation temperatures, applying a constant heating rate of t_1 (< 10 °C/s) until T_1 , were around 711 °C and 889 °C, respectively, and that the volume fraction of austenite achieved at the end of the soaking step, through lever rule, was approximately 35%, which means a partial austenitization of the material. The values found for Ac_1 and Ac_3 were close to the ones obtained through the continuous cooling transformation phase diagram of the material, where Ac_1 was 715 °C and Ac_3 was 870 °C. It is worth mentioning that during the continuous heating the dilatation curve presented two different stages: (i) from Ac_1 to T_c and (ii) from T_c to Ac_3 . In the first stage, the initial microstructure of the steel, consisting of ferrite and pearlite, started to change due to the recrystallization process and carbides dissolution. At T_c , the pearlite dissolution finished and the ferrite to austenite transformation started, with a gradual decrease of the relative change in length. This contraction due to austenite formation is a result of the competition between the phase transformation and the thermal expansion. The austenitization process completed when the Ac_3 temperature was reached, and beyond this temperature the sample was fully austenitized [15].

The resulting austenite decomposition during cooling, with a rate of t_2 (< 10 °C/s) until T_2 and a rate of t_3 (> 30 °C/s) until room temperature, showed the formation of ferrite, bainite and martensite, as disclosed in the Figure 7. In fact, it can be observed from the changes in the first derivative of change in length with respect to time that, for the respective rates mentioned, these phases started to form around 711 °C,

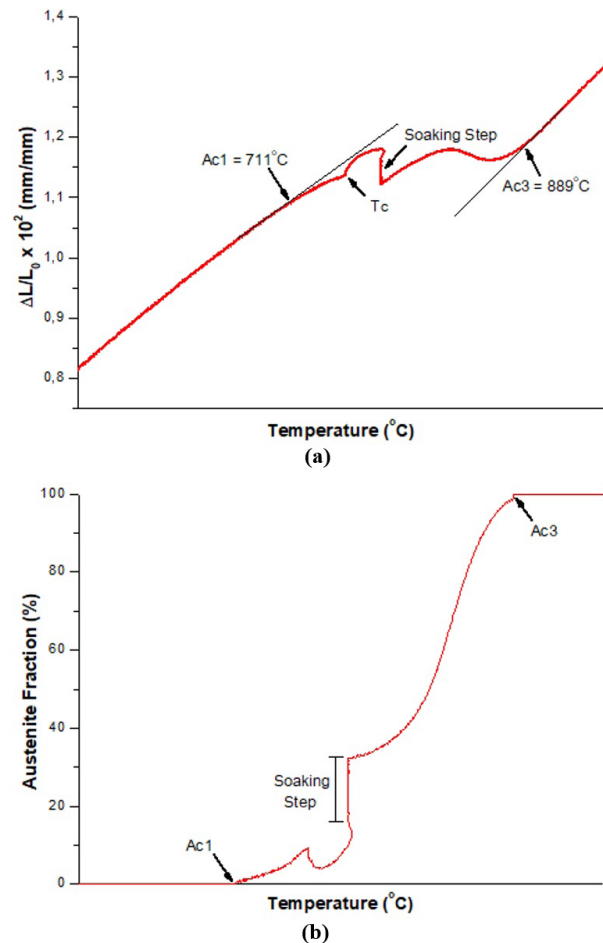


Figure 6. (a) Example of a dilatometric curve during the continuous heating, with a soaking step of ~80 s at T_1 . (b) Variation of austenite fraction for the applied heating cycle determined by the lever rule.

534 °C and 367 °C, respectively. Moreover, the volume expansion associated to bainite was minimal, which probably indicates a discrete volume fraction of this phase. Indeed, the microstructure evaluation through optical microscopy (Figure 8) was unable to verify, with good resolution, regions containing bainite as second phase, possibly because it was associated to martensite islands when it was formed.

3.2 Mechanical behavior

In general, the deformation behavior of a multi-phase microstructure is characterized by the deformation of each phase individually and the interaction between them [16]. The most common approach used to describe the tensile deformation behavior of a microstructure consisting of ferrite and martensite assumes a two phase system, in which the mechanical interactions arising from the constraints between the different phases bring about inhomogeneous distributions of stress and strain [17,18]. As cited by Byun and Kim [18], this inhomogeneous deformation may be related to plastic deformation of ferrite, accumulation of unrelaxed plastic incompatibility, plastic relaxation and

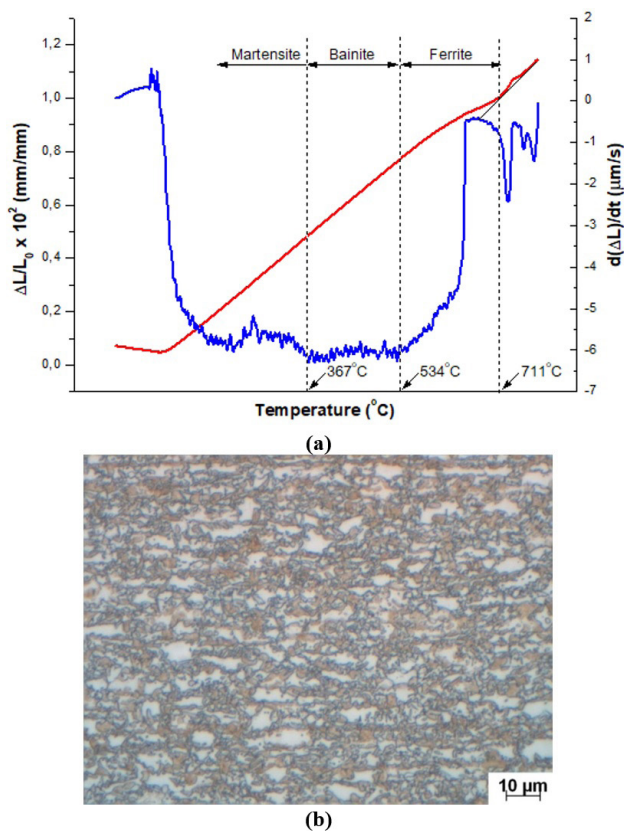


Figure 7. (a) Dilatometric curve and the first derivative of change in length with respect to time during the cooling step to evaluate the austenite decomposition after soaking at T_1 , where a rate of t_2 (< 10 $^\circ\text{C/s}$) was applied until T_2 and a rate of t_3 (> 30 $^\circ\text{C/s}$) was applied until room temperature. (b) Steel microstructure at the end of the test.

yielding of martensite. However, as previously mentioned and observed in this study, a significant amount of retained austenite can be found in the microstructure.

When present, this phase transforms to martensite during straining, and, due to the associated volume increase, serve as a source of dislocations, which will further increase the work hardening rate [19]. As a major effect, a delay of the plastic instability is observed, improving the steel ductility without significantly affecting its tensile strength. The result of this contributing factor in the tensile properties of the material is shown in Figure 8. For the three curves shown, the average values of yield strength, ultimate tensile strength, and total elongation were 512 ± 7 MPa, 1087 ± 1 MPa, and $17\% \pm 1\%$, respectively.

When compared to other steels with the same strength level, where usually a minimum elongation of 10% is required, an improvement of the material behavior is clear, which means a better structure for applications where good formability and strength are considered of interest.

4 Conclusions

The steel used in the present work showed a better strength-ductility combination when compared to other

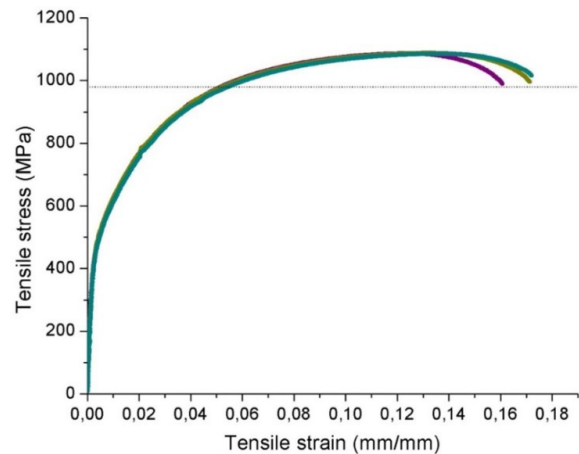


Figure 8. Engineering stress-strain curves of the tensile test specimens extracted from a Gleeble treated sample.

steels of the same strength level, where usually a minimum elongation of 10% is required. Its stress-strain curves showed that the average values found for yield strength, ultimate tensile strength, and total elongation were 512 ± 7 MPa, 1087 ± 1 MPa, and $17\% \pm 1\%$, respectively. This improvement of the material behavior is a result of the good microstructural features found in the final product, basically consisting of a homogeneous microstructure with martensite islands and retained austenite particles embedded in a ferrite matrix.

The volume fraction of the retained austenite, calculated through the Rietveld method in the XRD evaluation, was around 11%, and its carbon content corresponded to 0.81% w/w, which indicates some increase of ductility due to the TRIP effect during straining.

Additionally, the phase quantification method based on the pattern quality of the EBSD data revealed the presence of 27.3% of martensite and 68.7% of ferrite, which was quite close to the results obtained using the manual point counting method, 29.8% and 62.4%, respectively. However, regarding the retained austenite, this analysis showed a volume fraction of 4.1%, smaller than the value observed via XRD (11%). This difference is probably related to the spatial resolution limit of the SEM, to the smaller area of EBSD analysis, and to the transformation of the less stable austenite into the deformation induced martensite during the sample preparation.

For the study of the austenitization condition, it was observed that the starting and finishing transformation temperatures, for the applied heating rate of < 10 $^\circ\text{C/s}$, were around 711 $^\circ\text{C}$ and 889 $^\circ\text{C}$, respectively. The volume fraction of austenite formed at the end of a soaking step was approximately 35% and the decomposition of this austenite during cooling, with a rate of < 10 $^\circ\text{C/s}$ until an intermediate temperature and a rate of > 30 $^\circ\text{C/s}$ until room temperature, showed the formation of ferrite around 711 $^\circ\text{C}$, bainite at 534 $^\circ\text{C}$ and martensite below 367 $^\circ\text{C}$. It is noteworthy, though, that the volume expansion associated to bainite formation was minimal, which may indicate a discrete volume fraction of this phase.

References

- 1 Horvath CD. Advanced steels for lightweight automotive structures. In: Mallick PK, editor. *Materials, design and manufacturing for lightweight vehicles*. 2nd ed. Cambridge: Woodhead Publishing; 2021. p. 39-95.
- 2 Singh MK. Application of steel in automotive industry. *International Journal of Emerging Technology and Advanced Engineering*. 2016;6(7):246-253.
- 3 Galán J, Samek L, Verleysen P, Verbeken K, Houbaert Y. Advanced high strength steels for automotive industry. *Revista de Metalurgia*. 2012;48(2):118-131.
- 4 Nanda T, Singh V, Singh G, Singh M, Kumar BR. Processing routes, resulting microstructures, and strain rate dependent deformation behaviour of advanced high strength steels for automotive applications. *Archives of Civil and Mechanical Engineering*. 2021;7:1-24.
- 5 Kang J-Y, Park S, Moon M. Phase analysis on dual-phase steel using band slope of electron backscatter diffraction pattern. *Microscopy and Microanalysis*. 2013;19:13-16.
- 6 Chandrawanshi M, Singh RK, Sudharshan R. Development of high strength steel sheet with improved strain hardenability for automotive application. *Chernaya Metallurgiya = Izvestiya Ferrous Metallurgy*. 2019;62(9):827-832.
- 7 Soleimani M, Kalhor A, Mirzadeh H. Transformation-induced plasticity (TRIP) in advanced steels: a review. *Materials Science and Engineering A*. 2020;795(140023):1-14.
- 8 ASTM International. *ASTM A370: standard test methods and definitions for mechanical testing of steel products*. West Conshohocken: ASTM; 2011.
- 9 ASTM International. *ASTM E562: standard test method for determining volume fraction by systematic manual point count*. West Conshohocken: ASTM; 2019.
- 10 Bhadeshia HKDH, Edmonds DV. Analysis of mechanical properties and microstructure of high-silicon dual-phase steel. *Metal Science*. 1980;14(2):41-49.
- 11 Kang J, Kim DH, Baik S, Ahn T, Kim Y, Han HN, et al. Phase analysis of steels by grain-averaged EBSD functions. *ISIJ International*. 2011;51(1):130-136.
- 12 Wilson AW, Madison JD, Spanos G. Determining phase volume fraction in steels by electron backscattered diffraction. *Scripta Materialia*. 2001;45:1335-1340.
- 13 Ryde L. Application of EBSD to analysis of microstructures in commercial steels. *Materials Science and Technology*. 2006;22(11):1297-1306.
- 14 Wu J, Wray PJ, Garcia CI, Hua M, Deardo AJ. Image quality analysis: a new method of characterizing microstructures. *ISIJ International*. 2005;45(2):254-262.
- 15 Caballero FG, Capdevila C, García de Andres C. Modelling of kinetics and dilatometric behaviour of austenite formation in a low-carbon steel with a ferrite plus pearlite initial microstructure. *Journal of Materials Science*. 2002;37:3533-3540.
- 16 Ramos LF, Matlock DK, Krauss G. On the deformation behavior of dual-phase steels. *Metallurgical Transactions A, Physical Metallurgy and Materials Science*. 1979;10A:259-261.
- 17 Kim C. Modeling tensile deformation of dual-phase steel. *Metallurgical Transactions A, Physical Metallurgy and Materials Science*. 1988;19A:1263-1268.
- 18 Byun TS, Kim IS. Tensile properties and inhomogeneous deformation of ferrite-martensite dual-phase steels. *Journal of Materials Science*. 1993;28:2923-2932.
- 19 Sachdev AK. Effect of retained austenite on the yielding and deformation behavior of a dual phase steel. *Acta Metallurgica*. 1983;31(12):2037-2042.

Received: 21 July 2021

Accepted: 23 Nov. 2021